We are IntechOpen, the world's leading publisher of Open Access books Built by scientists, for scientists

4,800
Open access books available

122,000
International authors and editors

135M
Downloads

Our authors are among the

154
Countries delivered to

TOP 1%
most cited scientists

12.2%
Contributors from top 500 universities

CLARIVATE ANALYTICS BOOK CITATION INDEX INDEXED

WEB OF SCIENCE™

Selection of our books indexed in the Book Citation Index in Web of Science™ Core Collection (BKCI)

Interested in publishing with us?
Contact book.department@intechopen.com

Numbers displayed above are based on latest data collected.
For more information visit www.intechopen.com

15

Dynamic Responses of Composite Structures with Fluid-Structure Interaction

Young W. Kwon and Angela C. Owens
Naval Postgraduate School
USA

1. Introduction

As composite materials have been used for marine structures such as boats, ships, offshore structures, etc., the effect of FSI should be understood. In particular, FSI effect is expected to be significant for polymer composites because the water density is very comparable to the composites' densities. For example, the density of a carbon composite is approximately 50% greater than the water density. Sandwich composites consisting of very low densities of core materials have lower densities than that of water. As a result, the hydrodynamic mass associated with FSI would be very critical to composite structures under water. The growing use of composites in ship masts, superstructures, deck grates, piping, ducting, rudders, propellers, stacks, and various submarine structures requires extensive modeling and testing to help designers, builders and operators better understand composite response [Mouritz, et al., 2001].

These materials are subjected to a wide spectrum of loads during manufacturing and service life. Dynamic loadings, in particular, impact type event, represent a serious design concern for use of composite. Composite structures are more susceptible to impact damage than similar metallic structures which are more ductile in nature and can absorb typically large amounts of energy without failure. Furthermore, the damage in composites from impact can go undetected even when the mechanical properties may be drastically reduced from an impact. For these reasons, numerous experimental and analytical studies have been conducted to study the dynamic response of composites subjected to impact loading [Abrate, 1994; Aslan, et al., 2003; Kwon & Wojcik, 1998].

According to the review of past works, most of the research effort has been focused on low velocity impact damage, specifically, the damage predictions, and the evaluation and prediction of residual properties of damaged laminates. All of the research completed thus far has focused on damage in composites under impact loading in dry environments to support development of composites in aircraft structures.

As far as dynamic response of structures under water is concerned, a great deal amount of analytical and experimental studies have been conducted on the effect of fluid force on the natural frequencies, damping ratios and mode shapes of vibrating structures in contact with fluid. This is commonly known as the Fluid Structure Interaction (FSI) problem. FSI investigations have supported many problems in submarine signaling, offshore oil structure stability, and ship structure vibrations. Through these studies, many numerical and analytical methods have been developed in order to predict the added mass and the

resulting changes in natural frequency of a structure in contact with fluid. It has been determined and widely proven that the effect of fluid surrounding a structure decreases the natural frequency of a structure due to the increase in total kinetic energy of the vibrating structure and fluid from the addition of kinetic energy of the fluid. This effect can be interpreted as an added mass to the vibrating structure in the analysis of the dynamic response. Essentially as the structure vibrates, its mass is increased by the mass of the vibrating fluid with which it is in contact, consequently decreasing its natural frequency.

Studies of fluid structure interaction and the added mass effect, also known as virtual mass effect, hydrodynamic mass, and hydroelastic vibration of structures, started with Lamb [Lamb, 1921] who calculated the first bending mode of a submerged circular plate. In response to a problem of submarine signaling, Lamb investigated the vibrations of a thin elastic circular plate in contact with water. In his investigation he discovered that the natural frequencies for structures in contact with fluid are lower than the frequencies in air, based on the assumption that the modes shapes are virtually the same in water as in a vacuum. The resonant frequency was determined using Rayleigh's method. Lamb's theortical results were verified experimentally [Powell & Roberts, 1923]. Much later, more research was conducted for measuing and calculating natural frequencies of free vibartions of beams and plates under water [Lindholm, et al., 1965; Fu & price, 1979; Kwak, 1996]. Another branch of FSI studies is underwater explosion. Both experimental and numerical studies have been conducted for metallic structures [Kwon & Fox, 1993; Kwon, et al., 1994; Kwon & McDermott, 2001]. On the other hand, a much limited studies were undertaken for composite structures subjected to underwater explosion [Rasmussen, 1992; Rousseau, 1993; Mouritz, 1995, 1996; McCoy & Sun, 1997; Gong & Lam, 1998; and Lam, et al., 2003].

As far as impact loading on composite structures under water is concerned, the author's research team conducted the research for the first time, to our best knowledge [Kwon, 2009; Kwon & Kendall, 2009; Owen, et al., 2010]. This chapter presents both experimental work and numerical modeling and simulation of dynamics responses of composites subjected to impact loading as well as under water. The next section decsribes the fabrication of composite samples and the testing setup and procedure. Subsequently, experiental results are presented and discussed, followed by computational modeling and simulation of FSI to explain the experimental findings as well as to provide a series of parametric studies so that any important property or parameter can be identified in terms of the FSI effect. Conclusions are provided at the end.

2. Composite specimens and testing equipment

Three carbon fiber laminate samples are constructed for this study. Each sample is fabricated from TORAY T700CF carbon fiber bidirectional weave and DERAKANE 510-A vinyl-ester matrix resin. Each plate is fabricated through the Vacuum Assisted Resin Transfer Molding (VARTM) process, which consists of pulling resin through layers of carbon fibers using a vacuum pump. The plates consisted of eight plies oriented $[0/90/0/90]_s$ at 2.38 mm nominal thickness with dimensions of 457 x 457 mm. The DERAKANE resin is mixed with three hardeners, Methyl Ethyl Ketone Peroxide (MEKP), Cobalt Napthenate (CoNAP), and N-Dimethylaniline (DMA) to achieve a nominal 60 minute curing time. The hardeners are added solely to achieve proper gel time and do not affect composite strength. All resin components are mixed based on a percent weight for a nominal cure time per manufacturer's directions at

a temperature of less than 70ºF. The DERAKANE 510-A is measured by volume and the MEKP, CoNAP, and DMA are measured by weight.

Impact tests are conducted using a specially designed drop weight testing system, as shown in Fig. 1. This instrumented apparatus consists of a drop weight impactor, a load transducer, strain gages, high speed data analyzer, and an air box. The sample supporting fixture at the bottom of the drop tower is made of aluminum and facilitated square clamped conditions with a clear span of 305 x 305 mm. The composite plates are then clamped to the impactor frame using c-clamps to represent clamped boundary conditions. The transient response measurement of the sample includes force and strains as a function of time.

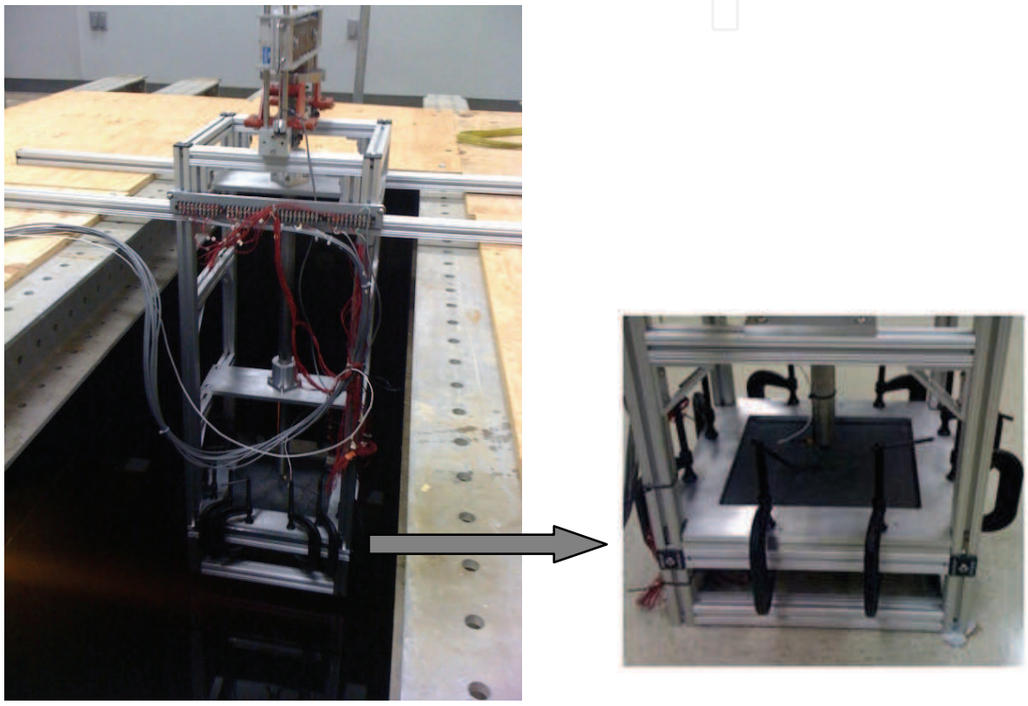

Fig. 1. Drop weight testing system in anechoic water tank

The drop weight impactor consists of a drop weight and an impact rod. The drop weight is supported by 4 steel guide rods, and the impact rod is supported by an aluminum frame base and a linear spring of spring constant 7508 N/m. The dimensions of the guide rods are 1.219 m high with a 6.35 mm diameter, and the dimensions of the base frame are 1.168 m high x 0.457 m wide x 0.457 m deep. The aluminum framing pieces and fasteners are designed and assembled for this research. The falling weight is guided by four small linear bearings. The impact rod is guided with two plain brushing aluminum linear bearings of 38.1 mm diameter enclosed in a casing for support. The top of the impact rod stays above the water surface so that the drop weight does not go into the water as it hits the impact rod on its top. It is important not to disturb the water during the impact testing so that a composite plate interacts with still water. The other end of the impact rod, which strikes a composite plate during impact, is located initially very close to the specimen surface inside the water such that the disturbance of water due to the impact rod is negligible. Therefore, FSI occurs only resulting from dynamic motion of composite plates.

A trigger at the base of the falling weight is used to measure data collection. The drop weight is kept constant at 12.0 kg. The impact rod is made of steel and has a mass of 12.7 kg. Impact energy can be varied by changing the drop height. The maximum height is 1.06 m, which can produce approximately 4.6 m/s initial velocity upon impact. The impact location is at the center of the composite sample. The selection of impact mass and height is made not to cause any damage to the composite plates so that transient dynamic response of the plates can be focused in the study.

The load cell used is an ICP® force sensor manufactured by PCB Piezotronics, Inc. which converts force into a measurable electrical output. The load transducer is mounted on the end of the impactor rod. The gage has an impact diameter of 15.88 mm. In the case of wet testing, the gages and cable connection are coated. The strain gages are three-element 45° single-plane rosettes, model CEA-00-250UR-350, by Vishay Micro-Measurements. There are four rosette strain gages bonded to each composite sample. The gages are bonded to the underside of the laminate samples, opposite side of impact, and waterproofed. Fig. 2 illustrates the orientation, location and designated x-y axis. Gage location #1 is directly at the center on the underside of the sample opposite the impact location. Gages #3 and #4 are placed along a diagonal line of the composite plate with Gage #4 at the quarter distance of the diagonal length. Gage #2 is located close to the vertical symmetric line of the center.

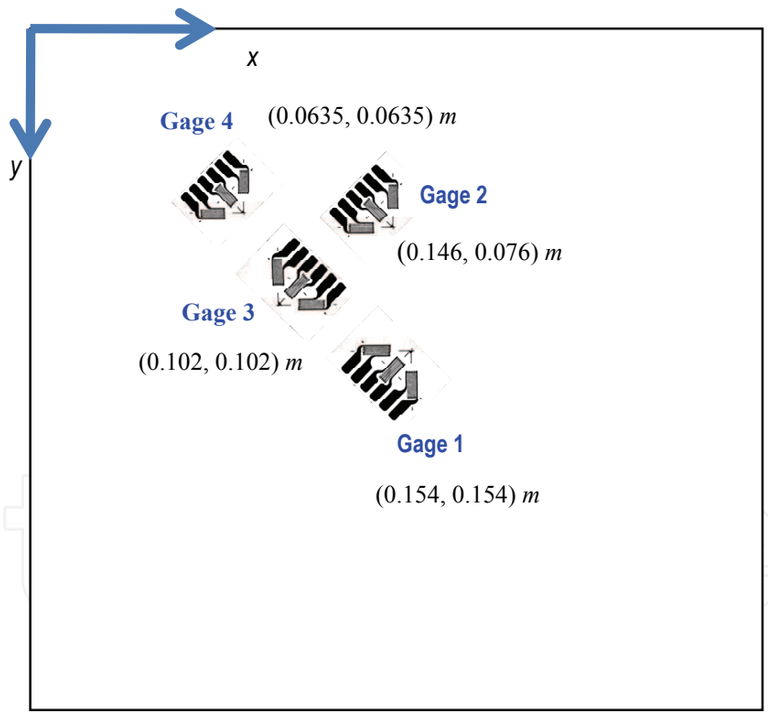

Fig. 2. Strain gage rosette locations opposite the side of impact.

Data acquisition is carried out using an acquisition system specifically developed for this project, that consists of a Pentium™ 4, 2.4 GHz, 512-MB RAM system, National Instruments™ simultaneous sampling multifunction DAQ, and five Vishay™ 2120 multi-channel strain signal conditioners. The system has a 16 bit analog-to-digital conversion resolution and is capable of reading a total of 16 channels at a throughput rate of up to 250 kS/s per channel, which is appropriate for the rate of testing used in this study. The data-

acquisition process is controlled using the NI-DAQmx driver software and LabVIEW™ interactive data-logging software that is specifically formatted for this research. A trigger located at the top of the impact rod is used to initiate data acquisition. Strain readings from four signal conditioners are multiplexed in order to accommodate all strain gages within the available number of channels. Errors due to instrumentation noise do not appear to cause problems in the data capture so no filtering is used.

An air box is specifically constructed to facilitate testing for air-backed wet environments. The box is made of 12.7 mm thick plexi-glass with dimensions 330 mm wide x 330 mm long x 127 mm deep. This box is then secured to the bottom aluminum support plate for the composite sample using 8 c-clamps of dimensions 76 mm jaw x 60 mm throat, and sealed with putty tape to prevent water leakage. The box completely covers the sample so that the bottom side of the plate is not exposed to water. A 19 mm diameter hole is cut out from the side to feed the wiring from the strain gages to the data analyzer, which is filled with putty to prevent water leakage during testing.

An anechoic water tank used for underwater surroundings testing is measured 2.75 m wide x 2.75 m long x 2.75 m deep. The anechoic tank is used to minimize the influence of the wave reflection from the boundary walls. The tank is filled with fresh water. A standing platform is constructed across the top of the tank made with aluminum I-beams and plywood, leaving a 0.635 m x 0.914 m square opening for suspension of the drop weight impactor.

3. Impact testing

Three different impact cases are studied in order to examine the effects of FSI on composite structures under dynamic loading. These cases are shown in Fig. 3. First, the dry impact is conducted as the baseline. For the dry impact test, the composite plates are impacted without having any contact with the water. This is shown in Fig. 3(a). Subsequent wet impact tests are undertaken for the same composite plates. In order to avoid any moisture effect on the composite materials, the wet impact testing is performed as soon as the composite plates are submerged into the anechoic water tank. Furthermore, once the wet impact testing is completed, dry impact of the plate is conducted just following the wet impact. The responses of the dry impact tests before and after the wet impact testing are compared. Their results are consistent. By doing so, it can be verified that the composite plates did not absorb any moisture to affect their material properties.

Two different wet impact conditions are considered. The first case has an air-containing rigid box attached to the bottom of the composite plates. The box is completely sealed so that no water permeates into the box when the composite plate with the attached box is submerged into the water of the anechoic water tank. Then, impact loading is applied to the composite plate submerged in water. This is called the air-backed wet impact and is shown in Fig. 3(b). The air-backed composite plate is only in contact with water at the top side where the impact occurs. The other wet impact case is very similar to the previous one except that the air-box is no longer sealed so that water fills the box when the plate and the box are put into the water tank. This is sketched in Fig. 3(c) and called the water-backed wet impact. The water-backed plate is exposed to water on both sides in this case. The same impact conditions, i.e. the same drop weight and height, are applied to the three impact loading cases. The wet impact responses are compared to the dry impact data in order to evaluate the FSI effects.

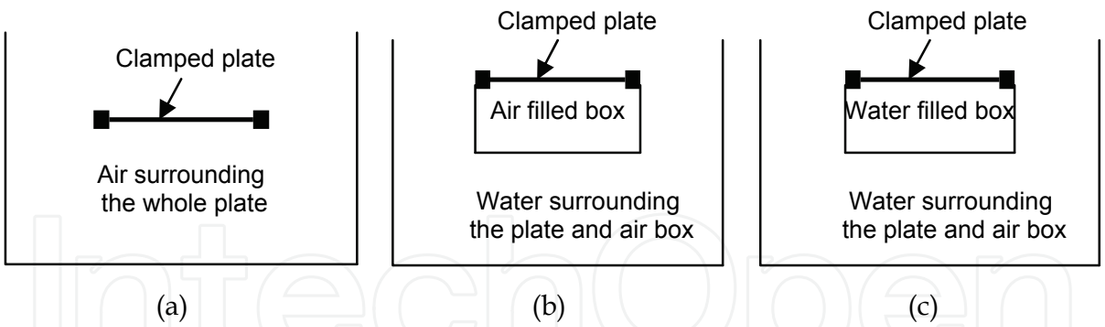

Fig. 3. Three different impact conditions with composite plates held in place: (a) dry impact, (b) air-backed wet impact, (c) water-backed wet impact

4. Experimental results

The impact test is conducted for the dry and wet composite plates. The mass of the free falling object is 12 *Kg* which is dropped from the height 1.06 *m*. In order to confirm the repeatability of the impact test data, every test condition is repeated several times for the same composite plate. The measured force and strain data are very close to one another. This fact confirms not only repeatability but also confirms there is no damage in the specimen. If damage occurred and accumulated in the composite plate, repeated testing would show different results with the damage. Figure 4 compares the two force data under the same dry impact condition. Other force data, which are not plotted here to avoid crowding, are very close to the graphs shown in the figure. In all figures unless otherwise mentioned, the force or strain plots are normalized in terms of the dry impact data so that the effects of FSI can be better represented in the plots.

The impact force is compared in Fig. 5 for the dry impact as well as the water-backed and air-backed wet impact cases. As shown in this figure, the air-backed and water-backed wet impacts yield 55% and 50% greater impact force than the dry case, respectively. The larger

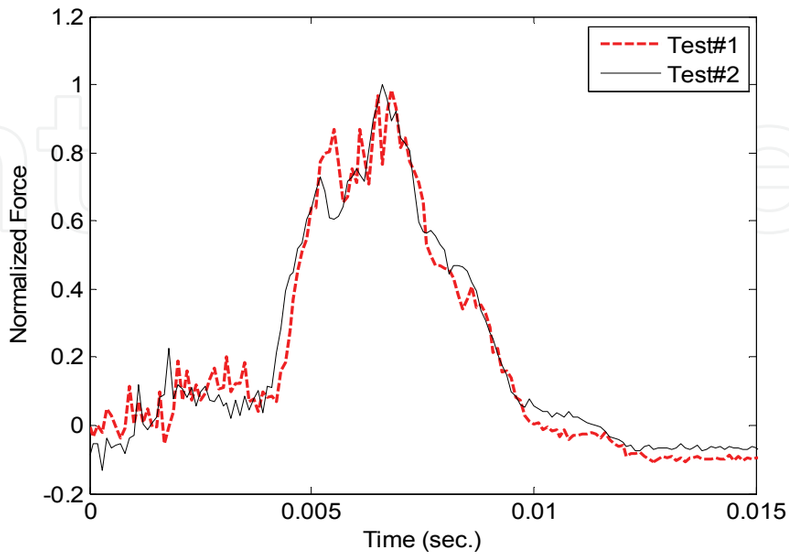

Fig. 4. Comparison of dry impact forces under the same impact condition

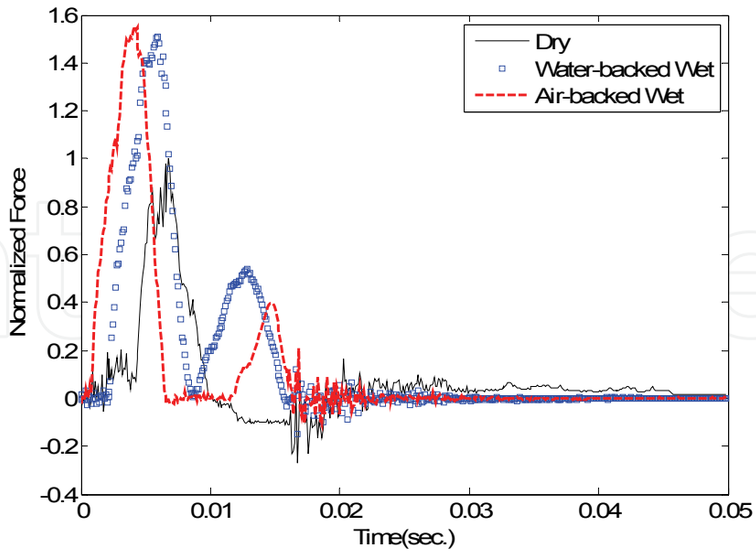

Fig. 5. Comparison of impact forces among dry, water-backed and air-backed wet impact cases

wet impact forces are caused by the hydrodynamic added mass effect. Because the mass of the composite plate is only 1.6 times greater than that of water, the plate with the added mass moves with a much slower velocity. As the plate moves more slowly, the contact force between the impactor and the plate becomes larger, which is recorded to the force gage. In order to support this argument, a series of finite element analyses is conducted in the next section.

Both wet impact forces have steep monotonic increases to their peak values just after the impactor hit the plates while the dry impact force shows an initial low plateau before it moves steeply to its peak value. Because the impactor is not held after the initial impact, it rebounds and lands again. As a result, both wet impacts show secondary peak forces. However, the dry impact does not have the secondary contact. In particular, the air-backed wet impact case gives a quite a delay between the initial and secondary impact forces while the water-backed wet impact case shows the secondary force occurring just after the initial one.

The reason that the air impact test does not produce the secondary impact is due to the spring in the impact test machine. The spring supports the impact rod which is supposed to hit the composite plate from a small distance above the plate before the impact loading. As the impact weight drops and hits the impact rod, the latter moves down with compression of the spring to strike the composite plate. For the air impact case, the initial impact force is lower than that for wet impact cases. Therefore, the redounding and landing force from the air impact is not large enough to overcome the spring force so that the rod cannot strike the plate again.

Because strain gage location #1 lies right underneath the impact site of the composite plate, the strains contain many higher frequency components compared to strains at other locations. A comparison of Fig. 5 to Fig. 6 shows that the peak values of impact forces and strains at position #1 occur simultaneously. Strains under wet impacts are more than double the dry impact strain at location #1. This ratio of peak strains between the wet and dry impacts is even greater than that of the impact forces.

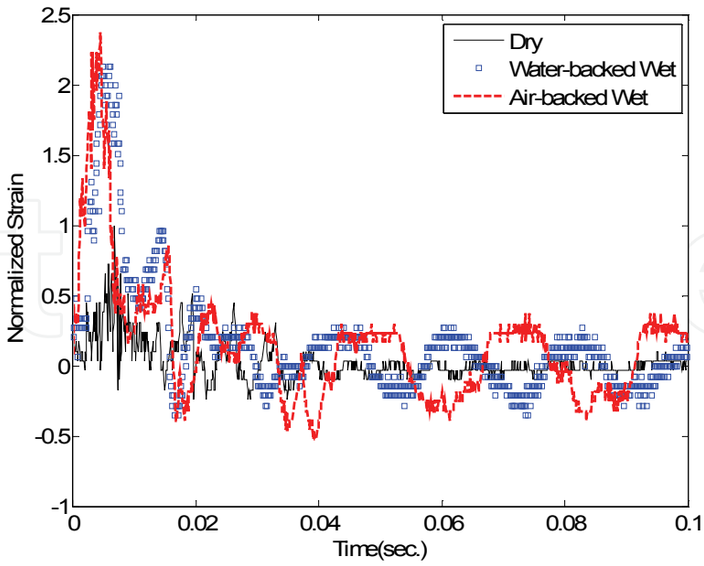

Fig. 6. Comparison of strains along x-axis at position #1 among dry, water-backed and air-backed wet impact cases

The differences between the wet and dry impact strains are smaller at the gage location #2 than those at the location #1. The strains under the air-backed wet impact are 20% and 50% greater than the dry impact strains along the x-axis and y-axis, respectively, as shown in Fig. 7. On the other hand, the water-backed impact results in 10% and 20% greater strains in the x-axis and y-axis, respectively, than the dry impact. The gage location #2 is closer to the clamped boundary in the y-axis direction. Thus, this suggests that the clamped boundary results in a greater FSI effect on the composite plate. Both wet impact strains show initial compressive strains before much larger tensile strains. Furthermore, these strain measurements show a clear difference among the response frequencies due to the added mass effect. Comparing the wet impact responses to the dry impact response, the response frequencies under the wet impacts are less than a half of the dry impact response frequency. Such a drastic reduction is caused by the light composite structure which is only about 1.6 times as heavy as the water. The response frequency is higher for the water-backed wet impact case than for the air-backed wet impact case by approximately 20%. This is an interesting result because the water-backed wet structure is expected to have a greater added mass effect with a lower response frequency. However, as expected, the decay of the strain peak values is greater for the water-backed wet impact case than the air-backed case. For example, the average damping ratio is 0.053, 0.062, and 0.11 for the dry, air-backed, and water-backed impact cases, respectively. This means the damping effect is the greatest for the water-backed case.

Calculation of the Added Virtual Mass Incremental Factor (AVMIF), β from Eq. (1) given below, yields approximately 6.5 and 11.5 for the water-backed and air-backed wet composite plates, respectively.

$$\frac{\omega_w}{\omega_d} = \frac{1}{\sqrt{1+\beta}} \tag{1}$$

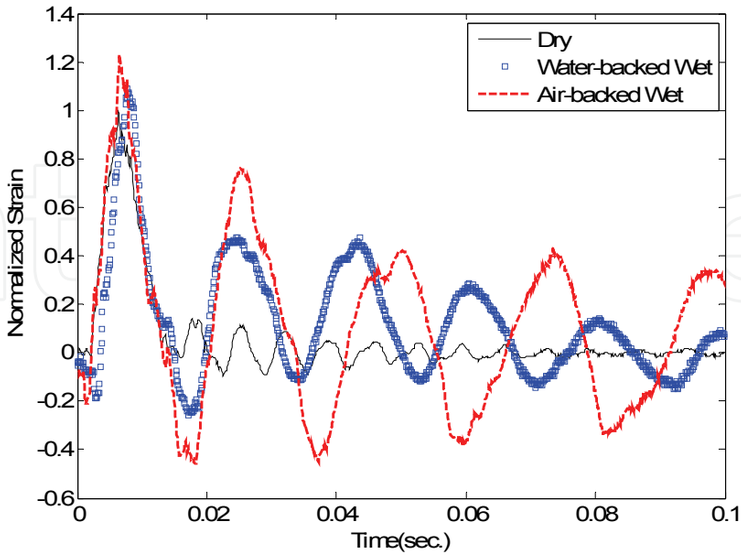

(a) Strain along x-axis

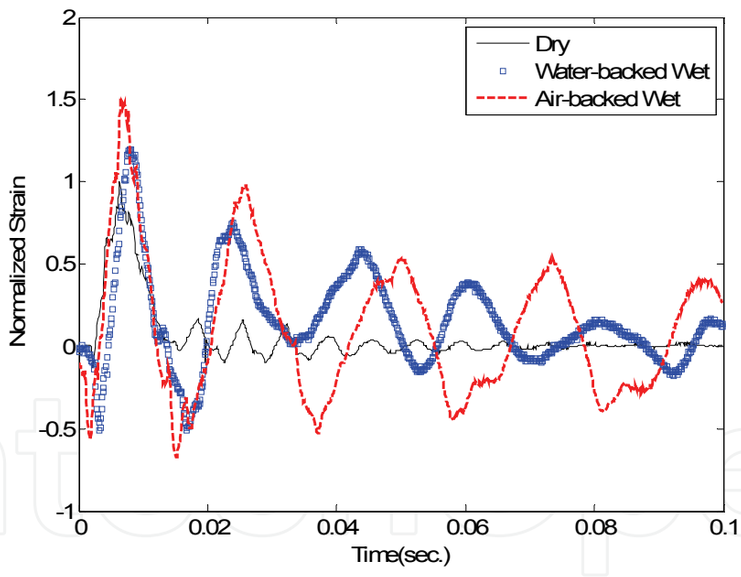

(b) Strain along *y*-axis

Fig. 7. Comparison of strains at position #2 among dry, water-backed and air-backed wet impact cases

where ω is the frequency and subscripts w and d denote the wet and dry cases, respectively. AVMIF represents the ratio of the kinetic energy of the water to that of the composite plate. The AVMIF for steel submerged in water ranges from 1.4 to 2.4 depending on the boundary conditions [Fu & Price, 1987; Haddara & Cao, 1996]. Comparison of AVMIF between the composite and steel shows clearly a much larger effect of FSI on the composite than steel.

The strain gage readings at gage location #3 have similar response characteristics as observed in the gage at location #2. Both air-backed and water-backed wet impacts resulted in 30% greater strains in x-axis than the dry impact. Because the gage location #3 is on the diagonal direction, strains in the y-axis were very close to those in the x-axis.

The effect of FSI is very significant for the strain gage reading at location #4, as shown in Fig. 8, and the strain readings are much less harmonic with more constraint effects from the clamped boundaries of the plate. First of all, both wet impact cases result in very large initial compressive strains compared to the dry impact case. The initial compressive strains are due to the clamped boundary conditions. After following the initial large compression, the air-backed wet impact case shows another large tensile strain while the water-backed case has a modest magnitude of tensile strain. The water on the backside of the water-backed composite plate seems to prevent further tensile strain at this gage location. The magnitudes of the strains at the gage location #4 are 4 to 5 times higher for the wet impact cases.

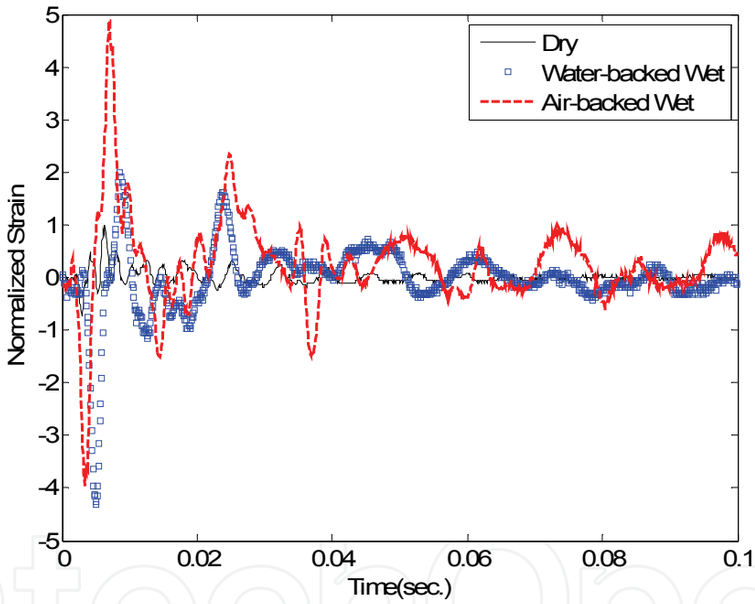

Fig. 8. Comparison of x-strains at position #4 among dry, water-backed and air-backed wet impact cases

In the next set of studies, the impact height is reduced to 0.76 m while the impact mass remains the same. This represents the impact energy reduction by 29%. Both dry and wet impact tests are undertaken with the reduced impact energy. Interestingly, as the impact energy is reduced, the peak forces under the dry and wet impacts are almost the same even though the force-time histories are different as shown in Fig. 9. However, comparison of strain responses between the dry and wet impact cases is similar between the two different impact energy conditions. For example, Figs. 10 and 11 are the strains at the gage locations #2 and #4.

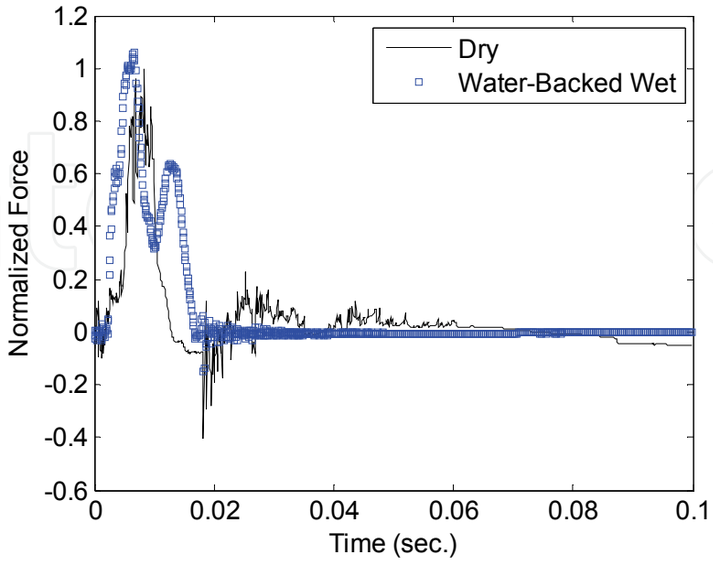

Fig. 9. Comparison of impact forces among dry and water-backed wet impact cases with a 29% reduced impact energy

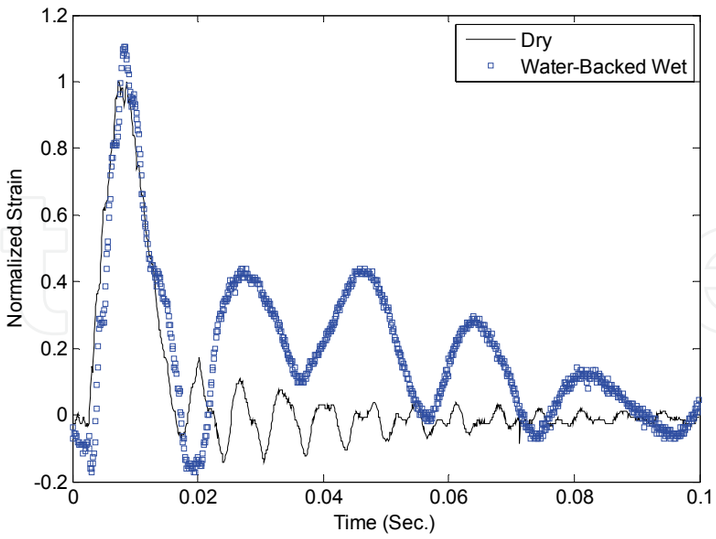

Fig. 10. Comparison of *x*-strains at position #2 among dry and water-backed wet impact cases with a 29% reduced impact energy

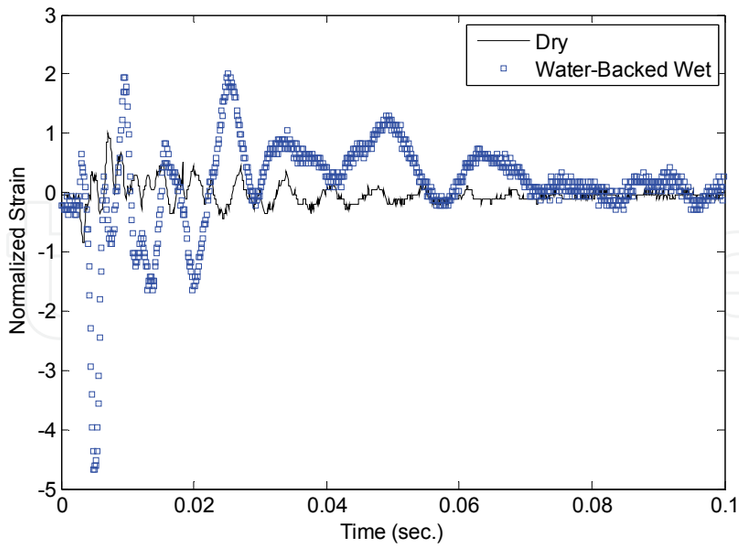

Fig. 11. Comparison of *x*-strains at position #4 among dry and water-backed wet impact cases with a 29% reduced impact energy

5. Computational modelling

A numerical study is conducted to confirm the experimental results at least qualitatively and to assess the effects of various parameters on FSI and impact loading. For the numerical study, 2-D modeling and analysis is conducted. Even though the experiments are 3-D, it is not believed the qualitative behavior would differ between 2-D and 3-D cases. The 2-D analysis is computationally much less time-consuming, especially with the FSI model containing a large domain of fluid.

The numerical model has a composite beam which has density 2000 Kg/m^3 and elastic modulus 50 GPa. The beam is 400 mm long, 20 mm wide, and 2 mm thick. Therefore, the composite has approximately twice density of water and is 40% lighter than aluminum and one quarter of steel. On the other hand, the elastic modulus is about 70% and 25% of those of aluminum and steel, common structural metals. As a parametric study, both density and elastic modulus of the beam are changed.

The computational model consists of both structure and fluid. Finite element formulations are developed for the FSI study. The beam is modeled using the Euler-Bernoulli beam theory. Because the beam is assumed to be very thin, the transverse shear deformation energy is negligible. The finite element matrix equation for the beam as well as for any general structure is expressed below:

$$[M_s]\{\ddot{d}\} + [C_s]\{\dot{d}\} + [K_s]\{d\} = \{F_e\} + \{F_{fs}\} \tag{2}$$

where $[M_s]$, $[C_s]$, and $[K_s]$ are the mass, damping and stiffness matrices of the structure, $\{d\}$ is the nodal displacement vector, $\{F_e\}$ and $\{F_{fs}\}$ are the force vectors from external loading and the fluid loading, respectively, In other words, the fluid loading comes from the FSI. Superimposed dot denotes the temporal derivative.

For the fluid medium, fluid viscosity was neglected and it was modeled as an acoustic medium. The velocity potential formulation was utilized for the acoustic medium, and it is derived here. The continuity equation is

$$\frac{\partial \rho}{\partial t} + \vec{\nabla} \cdot \rho \vec{u} = 0 \tag{3}$$

where ρ is the density, $\vec{u}$ is the velocity vector, $\vec{\nabla}$ is the gradient operator, and t indicates time. The change of density is expressed as

$$\rho = \rho_o (1 + s) \tag{4}$$

in which s is called condensation and ρ_o is an ambient fluid density. Substitution of Eq. (4) into Eq. (3) with an assumption of $s \ll 1$ yields

$$\frac{\partial s}{\partial t} + \vec{\nabla} \cdot \vec{u} = 0 \tag{5}$$

The force-balance equation is

$$\rho_o \frac{\partial \vec{u}}{\partial t} = -\vec{\nabla} p \tag{6}$$

where p is the pressure. A scalar field called the velocity potential is defined as follows:

$$-\vec{u} = \vec{\nabla} \varnothing \tag{7}$$

Replacing the velocity by the velocity potential in Eq. (6) results in

$$\vec{\nabla}\left(-\rho_o \frac{\partial \varnothing}{\partial t} + p \right) = 0 \tag{8}$$

The relationship $p = Bs$ as well as Eq. (7) are substituted into Eq. (5) to give

$$\frac{I}{B} \frac{\partial p}{\partial t} - \nabla^2 \varnothing = 0 \tag{9}$$

where B is the fluid bulk modulus. Elimination of pressure from Eqs. (8) and (9) yields the final wave equation in terms of the velocity potential.

$$\frac{1}{c^2} \ddot{\varnothing} - \nabla^2 \varnothing = 0 \tag{10}$$

in which $c^2 = B / \rho_o$ and c is the speed of sound. In order to apply Eq. (10) to FSI problems, the velocity at the FSI interface boundary is computed from the structural dynamics, i.e. Eq. (2), and it is applied to the wave equation through Eq. (7). On the other hand, the fluid pressure is computed from the wave equation using

$$p = \rho_o \frac{\partial \varnothing}{\partial t} \tag{11}$$

The acoustic wave equation is processed using the Galerkin method to formulate the finite element matrix equation. The resulting matrix equation for the wave equation is expressed as

$$\frac{1}{C^2}\left[M_{\mathrm{f}}\right]\left\{\ddot{\varnothing}\right\}+\left[K_{\mathrm{f}}\right]\left\{\varnothing\right\}=\left\{\mathrm{F}_{\mathrm{f}}\right\} \tag{12}$$

where

$$\left[M_f\right]=\int_{\Omega^f}[H]^T\left[H\right]d\Omega \tag{13}$$

$$[K_f]=\int_{\Omega^f}[\vec{\nabla}H]^T[\vec{\nabla}H]d\Omega \tag{14}$$

$$\{F_f\}=\int_{\Gamma^f}[H]^T u_n d\Gamma \tag{15}$$

Here, [H] the a vector of shape functions. For the present analysis, four-node quadrilateral elements are used for the fluid acoustic model. In addition, Ω^f and Γ^f are the fluid domain and boundary, respectively, and u_n is the fluid velocity normal to the boundary.
For an FSI application, Eqs. (2) and (12) are solved in a staggered matter. For example, the structural analysis is conducted using Eq. (2). Then, the structural velocity at the FSI boundary is computed. From the velocity compatibility condition, both structural and fluid velocities must be the same at the FSI boundary. For an inviscid flow, only the normal velocity components are considered for the compatibility condition. As a result, Eq. (15) is computed from the fluid velocity at the FSI interface and the fluid analysis is performed from Eq. (12). From the fluid analysis, fluid pressure is computed at the FSI interface. From the force equilibrium, the fluid pressure is used as an applied force to the structure. This completes one cycle and the whole process continues as the time increases. For an efficient computation, the explicit time integration technique was used for both structural and fluid analyses. For example, time integration of fluid analysis is conducted as below and similarly for structural analysis.

$$\left\{\ddot{\varnothing}\right\}^t=\left[K_{\mathrm{f}}\right]\left\{\varnothing\right\}=[M_f]^{-1}\ \{\{F_f\}^t-\left[K_{\mathrm{f}}\right]\left\{\varnothing\right\}^t\} \tag{16}$$

$$\left\{\dot{\varnothing}\right\}^{t+\frac{\Delta t}{2}}=\left\{\dot{\varnothing}\right\}^{t-\frac{\Delta t}{2}}+\Delta\mathrm{t}\{\ddot{\varnothing}\}^{\mathrm{t}} \tag{17}$$

$$\left\{\varnothing\right\}^{t+\Delta t}=\left\{\varnothing\right\}^t+\Delta t\{\dot{\varnothing}\}^{\mathrm{t}+\frac{\Delta \mathrm{t}}{2}} \tag{18}$$

6. Numerical results

First of all, the impact force is computed from the models described in the previous section and compared between dry and wet impact cases in Fig. 12. The computer modeling and simulation with an impact energy of 0.5J produced a result qualitatively agreeing with the experimental observation as plotted in Fig. 5. Because of FSI, the wet impact results in a

higher impact force than the dry impact. The FSI produces an added mass effect, which makes the structure under water move slower than the same structure in air. Such a slower movement yields a higher contact force between the impactor and the structure.

A parametric study is conducted to study the effect of different material properties on the peak impact force ratios between the wet and dry impacts. The first parameter is the structural mass density. As shown in Fig. 13, the structural density significantly affects the wet impact force. As the structural mass density becomes smaller and more comparable to the water density, the added mass effect gets greater. Therefore, the peak of the wet impact

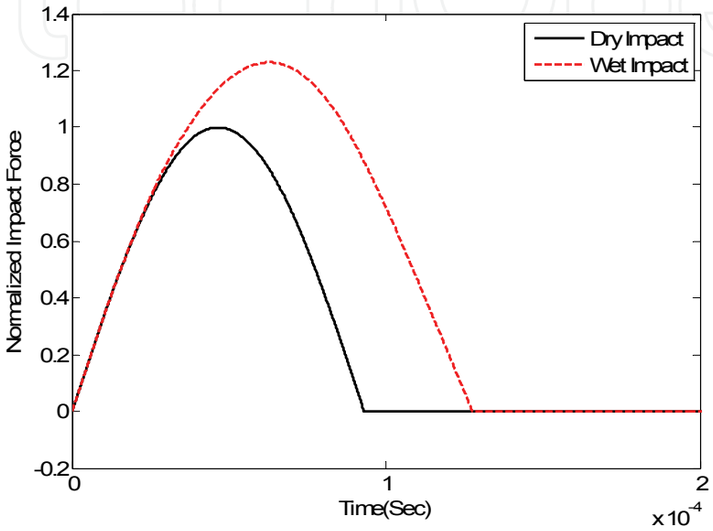

Fig. 12. Comparison of normalized impact forces between dry and wet impact modeling of a composite beam

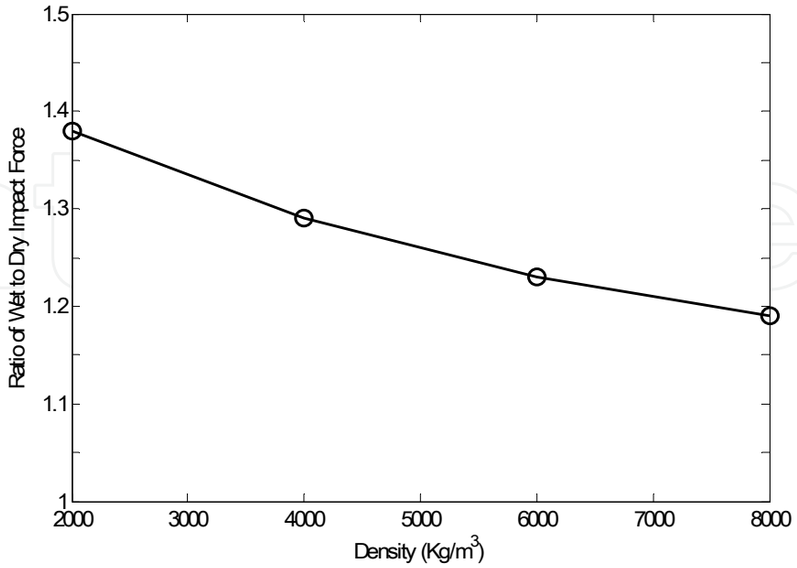

Fig. 13. Plot of effects of beam density on ratios of peak impact forces between wet and dry impact models

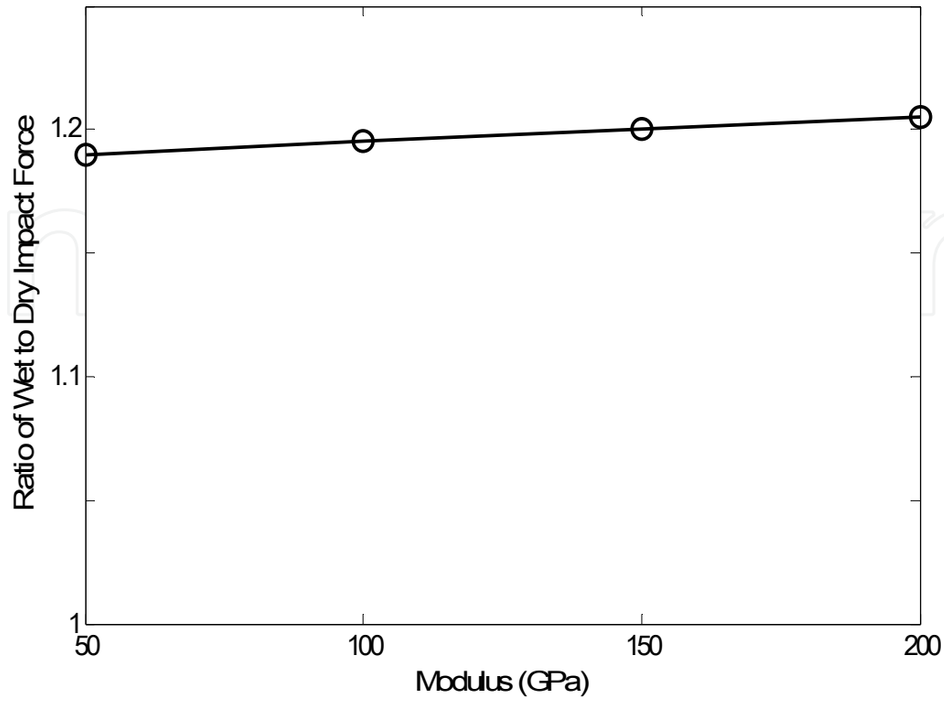

Fig. 14. Plot of effects of beam elastic modulus on ratios of peak impact forces between wet and dry impact models

becomes much greater than that of the dry impact for a lighter structure. This suggests that wet impact is more critical for polymer composite structures than metallic structures because polymer composites have much lower mass densities than conventional metals. On the other hand, a change of elastic modulus of the structure has only a minor effect on the wet impact force as shown in Fig. 15. In other words, the ratio of the wet to dry peak impact forces does not vary much with respect to the change of structural modulus.

Because the previous experimental study also indicates the ratio of the peak impact force between the wet and dry impacts is affected by the impact energy, as the impact energy becomes smaller, the FSI effect also becomes lower so that the impact force ratio approaches unity. This fact is also supported from the numerical study. In the numerical simulation, the impact mass is varied in the finite element model in order to change the impact energy. The maximum contact force under wet impact loading is computed for different impact energy (i.e. impact mass) and the value is normalized in terms of the maximum contact force under dry impact with the same impact energy. The results are plotted in Fig. 16. As shown in the figure, the impact force ratio approaches to unity as the impact mass becomes 0.001.

Another application of the computer model is to investigate the effect of FSI under impact loading on the strain histories of the structure. Because the FSI effect is not uniform, the experimental study indicates that the strain near to the boundary is more influenced by the FSI effect. This fact is also investigated using the numerical model. Fig. 16 shows the locations of the beam where the strains are computed. Figures 17 though 20 plot the strain histories of the wet and dry impacts, respectively. The plots are normalized with respect to

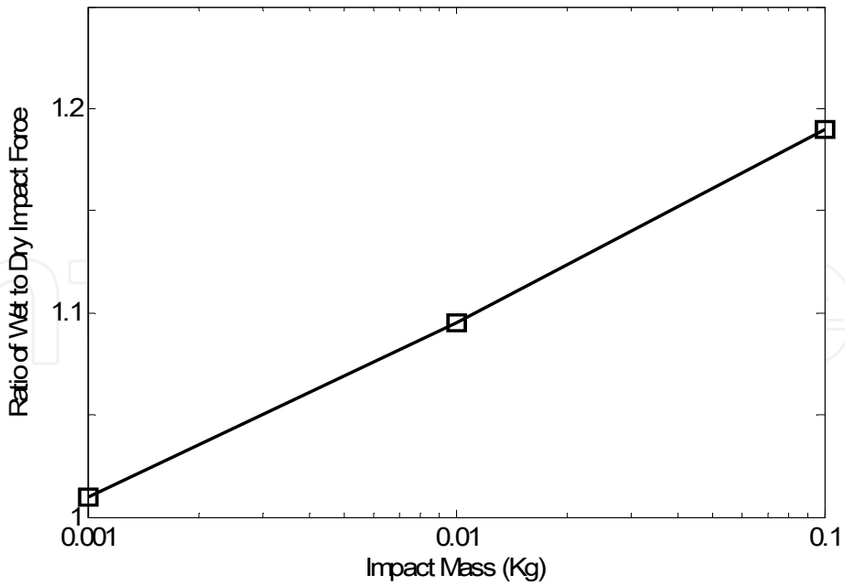

Fig. 15. Plot of effects of impact mass on ratios of peak impact forces between wet and dry impact models

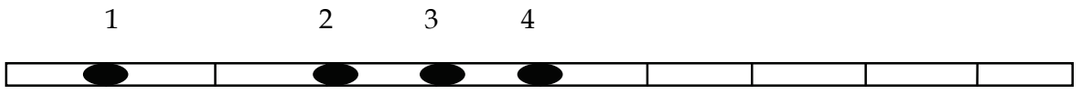

Fig. 16. Location of strain calculations along the clamped beam model

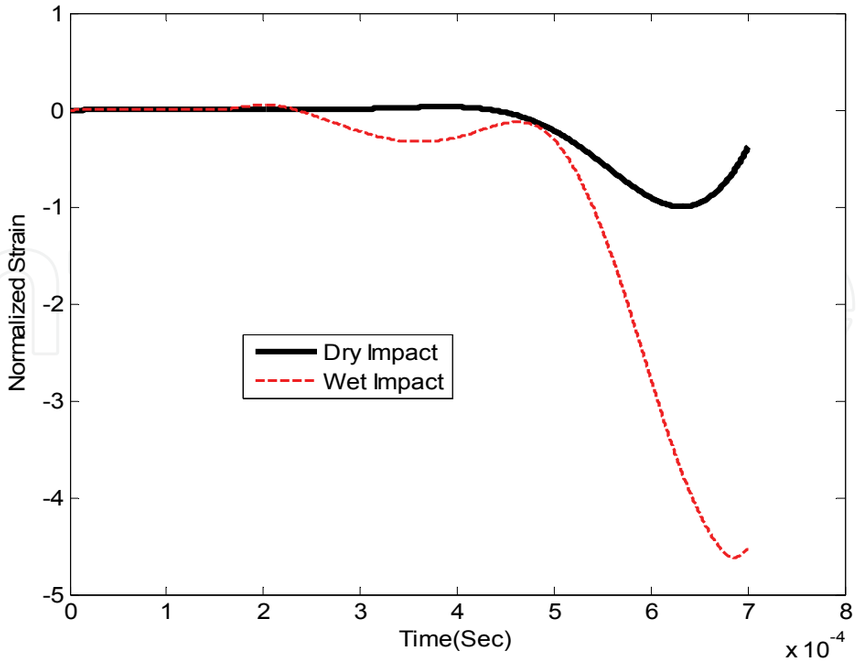

Fig. 17. Strain time history at Location 1 of Fig. 16 (beam model)

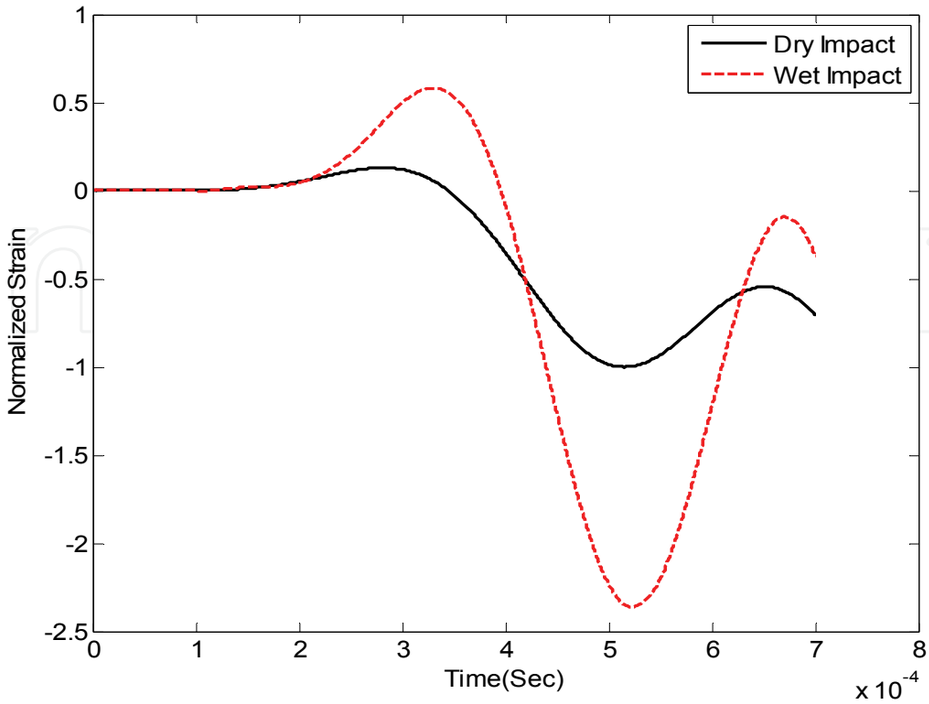

Fig. 18. Strain time history at Location 2 of Fig. 16 (beam model)

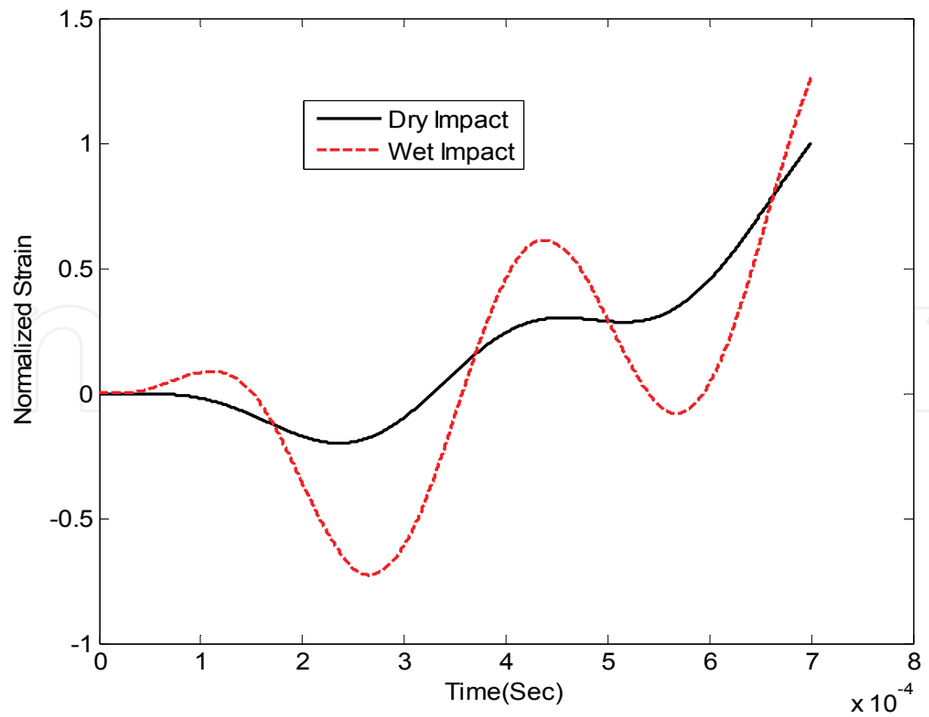

Fig. 19. Strain time history at Location 3 of Fig. 16 (beam model)

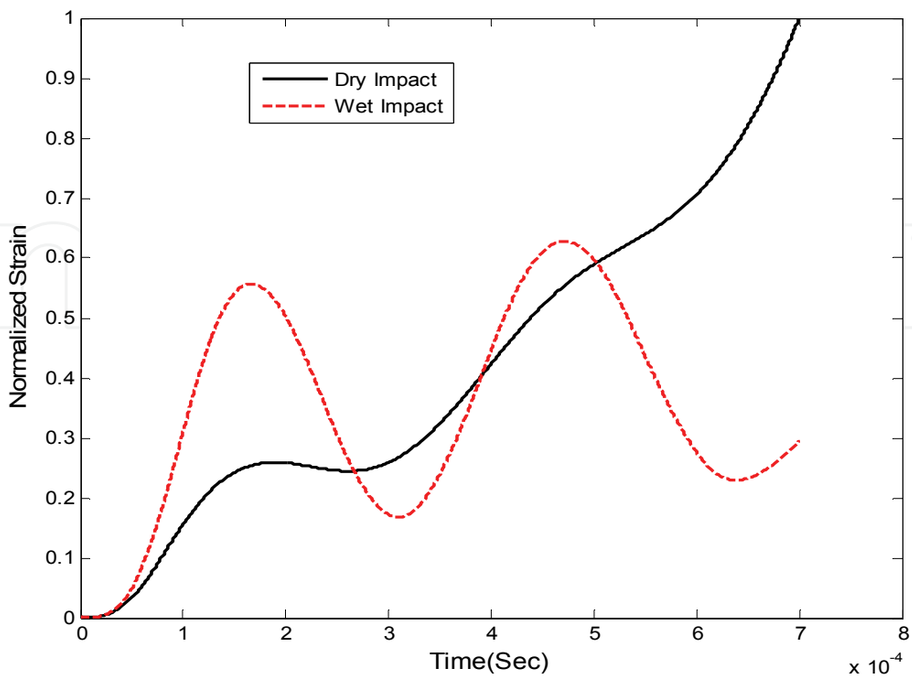

Fig. 20. Strain time history at Location 4 of Fig. 16 (beam model)

the respective dry impact strain. Comparing those strains tells clearly Location 1 has the greatest difference of strain histories between the wet and dry impacts. In other words, the FSI effect with impact loading is greater at the location near to the clamped boundary.

7. Conclusion

Both experimental and numerical studies are conducted to understand the effect of FSI with impact loading on polymer composite structures. For an experimental study, an experimental set-up is designed and fabricated for impact testing on composite plates submerged in water. In order to investigate the transient dynamic response of composite plates with FSI effects under impact loading; three impact conditions, dry, air-backed wet, and water-backed wet impact conditions are considered, respectively. In order to focus on the FSI effects on the transient dynamic responses, impact loading is controlled not to cause any damage to the composite plates. Since the composite material has a very comparable density to water, the FSI effects are very significant on the impact force and transient responses of the plates. Due to the added mass effect of water, the impact force is much greater for the wet impact cases than for the dry impact. Similarly, wet impact produces much greater transient strains on the composite plates. As a result, the wet impact is more detrimental to the structure than the dry impact. However, the increase of magnitude of transient strain responses resulting from the FSI with wet impacts varies significantly. The transient strain responses depend on the location of the composite plate because the added mass effect is not uniform over the plate. The location near to the clamped boundary corner has generally a greater FSI effect on the transient strain response. Comparison of AVMIF

between the composite and steel shows approximately 3 to 5 time greater values for composites than steel, which indicates a much greater effect of FSI on the composite than steel.

The numerical modeling and simulation confirms the experimental observation. Wet Impact loading on a composite structure produces a much greater impact force than dry impact. However, as the impact energy becomes smaller, the peak wet impact force becomes closer to that of the dry impact force. A numerical parametric study also indicates that density of the structure significantly influences the FSI effect of the wet impact. If an impacted structure has a low density like a polymer composite, the FSI effect on impact loading is larger while the effect is less for a structure made of a conventional metal. On the other hand, the elastic modulus of the structure has a negligible change in the FSI effect with impact loading. Furthermore, both experimental and computational studies show that the FSI effect with impact loading is not uniform and greater near to the clamped boundary.

8. Acknowledgement

The authors acknowledge the assistances from T. Christian and J. Mobley for preparing the impact testing equipment; and P. K. Kendall, A. S. Kwon, S. Blair, J. M. Didoszak for assisting with the computational work. They also express sincere thanks to the sponsorship by ONR and NSWC-CD.

9. References

Abrate, S., (1994). Impact on laminated composites; recent advances, *Applied Mechanics Reviews*, Vol. 47, No. 11, pp. 517-544.

Aslan, Z.; Karakuzu, R. & Okutan, B., (2003). The response of laminated composite plates under low-velocity impact loading, *Composites Structures*, Vol. 59, pp. 119–127.

Fu, Y. & Price, W. G., (1987). Interactions between a partially or totally immersed vibrating cantilever plate and the surrounding fluid, *Journal of Sound and Vibration*, Vol. 118, No. 3, pp. 495–513.

Gong, S. W. & Lam, K. Y., (1998). Transient response of stiffened composite submersible hull subjected to underwater explosive shock,, *Composite Structures*, Vol. 41, No. 1, pp. 27-37.

Haddara, M. R. & Cao, S., (1996). A study of the dynamic response of submerged rectangular flat plates, *Marine Structures*, Vol. 9, pp. 913–933.

Kwak, M. K., (1996). Hydroelastic vibration of rectangular plates, *Journal of Applied Mechanics*, Vol. 63, pp. 110–115.

Kwak, M. K. & Kim, K. C., (1991). Axisymmetric vibration of circular plates in contact with fluid, *Journal of Sound and Vibration*, Vol. 146, pp. 381–389.

Kwon, Y. W., (2009). Study of fluid effects on dynamics of composite structures, (PVP2009-77982), *2009 ASME Pressure Vessel and Piping Conference*, Prague, Czech Republic, July.

Kwon, Y. W.; Bergensen, J. K. & and Shin, Y. S., (1994). Effect of surface coatings on cylinders exposed to underwater shock, *Journal of Shock and Vibration*, Vol. 1, No. 3, pp. 637-646.

Kwon Y. W. & Cunningham, R. E., (1998). Comparison of USA-DYNA finite element models for a stiffened shell subject to underwater shock", *Computers and Structures*, Vol. 66, No. 1, pp. 127-144.

Kwon Y. W. & Fox, P. K.,(1993). Underwater shock response of a cylinder subjected to a side on explosion, *Computers and Structures*, Vol. 48, No. 4, pp. 637-646.

Kwon Y. W. & Kendall, P. K., (2009). Fluid-structure interaction of composite structures subjected to dynamic loading", *First Joint ASC and CACSMA Conference*, September 15-17, Newark, Delaware.

Kwon, Y. W. & McDermott, P. M., (2001). Effects of void growth and nucleation on plastic deformation of plates subjected to fluid-structure interaction", *ASME Journal of Pressure Vessel Technology*, Vol. 123, November, pp. 480-485

Kwon, Y. W. & Wojcik, G. W., (1998). Impact Study of Sandwich Composite Structures with Delamination, *Journal of Composite Materials*, Vol. 32, No. 5, pp. 407-430.

Lam, K. Y.; Zong, Z. & and Wang, Q. X., (2003). Dynamic Response of a Laminated Pipeline on the Seabed Subjected to Underwater Shock, *Composites Part B: Engineering*, Vol. 34, pp. 59-66.

Lamb, H., (1921). On the vibrations of an elastic plate in contact with water, *Proceeding of the Royal Society (London)*, Vol. A 98, pp. 205–216.

Lindholm, U. S.; Kana, D. D. & Chu, W. H., (1965). Elastic vibration characteristics of cantilever plates in water, *Journal Ship Research*, Vol. 9, No. 1, pp. 11–22.

McCoy, W. & Sun, C. T., (1997). Fluid-structure interaction analysis of a thick-section composite cylinder subjected to underwater blast loading, *Composite Structures*, Vol. 37, No. 1, pp. 45-55.

Mouritz, A. P., (1995). The damage to stitched GRP laminated by underwater explosion shock loading", *Composite Science and Technology*, Vol. 55, pp. 365-373.

Mouritz, A. P., (1996). The effect of underwater explosion shock loading of the flexural properties of GRP laminates, *Int. J. Impact Engng*, Vol. 18, No. 2 pp. 129-139.

Mouritz, A. P.; Gellert, E.; Burchill, P. & Challis, K., (2001). Review of advanced composite structures for naval ships and submarines, *Composite Structures*, Vol. 53, pp. 21-41.

Owens, A.C.; Didoszak, J. M.; Kwon, A. S. & Kwon, Y. W., (2010). Underwater impact of composite structures, (PVP2010-25065) *2010 ASME Pressure Vessel and Piping Conference*, Bellevue, Washington, July.

Powell, J. H. & Roberts, J. H. T., (1923). On the frequency of vibration of circular diaphragms, *Proceeding of the Royal Society (London)*, Vol. 35, pp. 170–182.

Rasmussen, E. A., (1992). Underwater Shock Testing and Analysis of Composite Cylinders, *Shock and Vibration Symposium*, 1992.

Rousseau, M. P.; Kwon, Y. W. & Shin, Y. S., (1993). Modeling the fffects of shock on an underwater composite cylinder", *64th Shock & Vibration Symposium*, Ft. Walton Beach, FL, Oct.

Volcy, G. C.; Morel, P. & Bureau, M., (1979). Some studies and research related to the hydro-elasticity of steel work, *Proceedings of the 122nd Euromech Colloquium on numerical analysis of the dynamics of ship structures,* pp. 403-406.

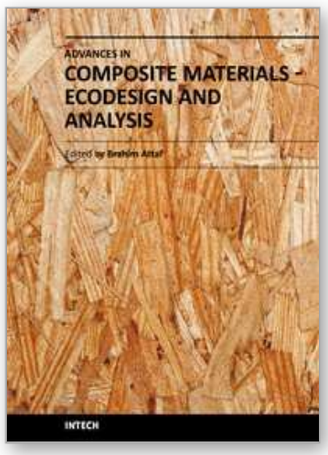

Advances in Composite Materials - Ecodesign and Analysis
Edited by Dr. Brahim Attaf

ISBN 978-953-307-150-3
Hard cover, 642 pages
Publisher InTech
Published online 16, March, 2011
Published in print edition March, 2011

By adopting the principles of sustainable design and cleaner production, this important book opens a new challenge in the world of composite materials and explores the achieved advancements of specialists in their respective areas of research and innovation. Contributions coming from both spaces of academia and industry were so diversified that the 28 chapters composing the book have been grouped into the following main parts: sustainable materials and ecodesign aspects, composite materials and curing processes, modelling and testing, strength of adhesive joints, characterization and thermal behaviour, all of which provides an invaluable overview of this fascinating subject area. Results achieved from theoretical, numerical and experimental investigations can help designers, manufacturers and suppliers involved with high-tech composite materials to boost competitiveness and innovation productivity.

INTECH
open science | open minds

InTech Europe
University Campus STeP Ri
Slavka Krautzeka 83/A
51000 Rijeka, Croatia
Phone: +385 (51) 770 447
Fax: +385 (51) 686 166
www.intechopen.com

InTech China
Unit 405, Office Block, Hotel Equatorial Shanghai
No.65, Yan An Road (West), Shanghai, 200040, China
中国上海市延安西路65号上海国际贵都大饭店办公楼405单元
Phone: +86-21-62489820
Fax: +86-21-62489821

IntechOpen